Novel targets in the liver to treat cardiometabolic diseases

Ge, X.

CHAPTER 2

Inhibition of DHCR24 activates LXRα to ameliorate hepatic steatosis and inflammation

Enchen Zhou, Xiaoke Ge, Hiroyuki Nakashima, Rumei Li, Hendrik J.P. van der Zande, Cong Liu, Zhuang Li, Christoph Müller, Franz Bracher, Yassene Mohammed, Jan Freark de Boer, Folkert Kuipers, Bruno Guigas, Christopher K. Glass, Patrick C.N. Rensen, Martin Giera, Yanan Wang

EMBO Mol Med 2023, 5: e16845

Abstract

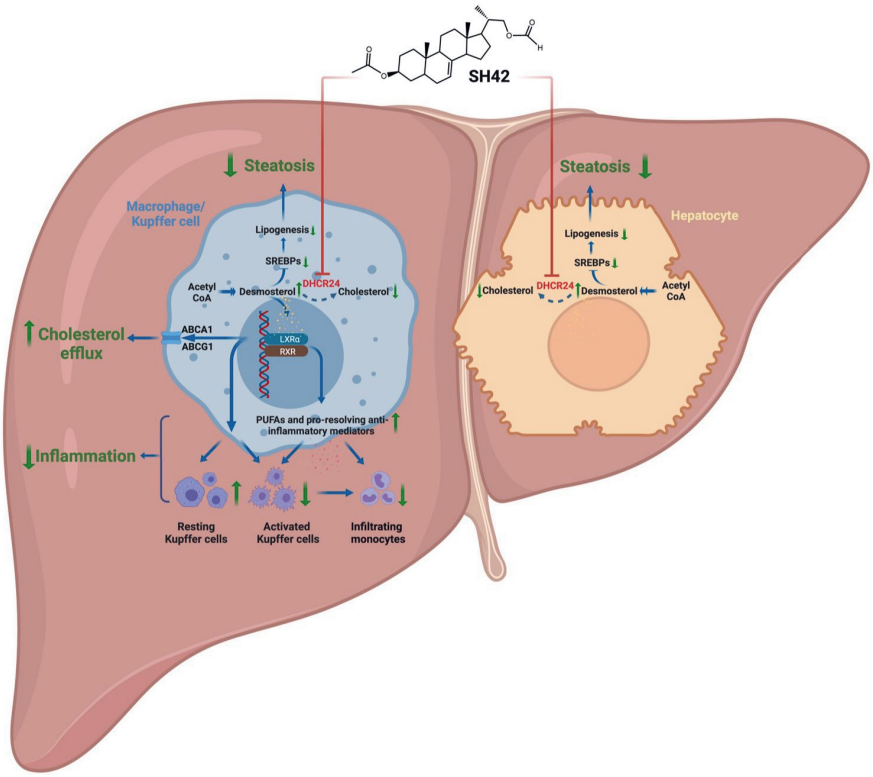

Liver X receptor (LXR) agonism has theoretical potential for treating NAFLD/NASH but synthetic agonists induce hyperlipidemia in preclinical models. Desmosterol, which is converted by Δ24-dehydrocholesterol reductase (DHCR24) into cholesterol, is a potent endogenous LXR agonist with anti-inflammatory properties. We aimed to investigate the effects of DHCR24 inhibition on NAFLD/NASH development. Here, by using APOE*3-Leiden.CETP mice, a well-established translational model that develops diet-induced human-like NAFLD/NASH characteristics, we report that SH42, a publishedDHCR24 inhibitor, markedly increases desmosterol levels in liver and plasma, reduces hepatic lipid content and the steatosis score, and decreases plasma fatty acid and cholesteryl ester concentrations. Flow cytometry showed that SH42 decreases liver inflammation by preventing Kupffer cell activation and monocyte infiltration. LXRα-deficiency completely abolishes these beneficial effects of SH42. Together, inhibition of DHCR24 by SH42 prevents diet-induced hepatic steatosis and inflammation in a strictly LXRα–dependent manner without causing hyperlipidemia. Finally, we also showed that SH42 treatment decreased liver collagen content and plasma alanine transaminase levels in an established NAFLD model. In conclusion, we anticipate that pharmacological DHCR24 inhibition may represent a novel therapeutic strategy for treatment of NAFLD/NASH.

Introduction

Non-alcoholic fatty liver disease (NAFLD) comprises a spectrum of diseases ranging from simple hepatic steatosis to non-alcoholic steatohepatitis (NASH). The latter is characterized by steatosis, hepatocellular damage and inflammatory cell infiltration with or without fibrosis. Hepatic steatosis is defined as accumulation of primarily neutral lipids such as triacylglycerols (TAG) and cholesteryl esters (CE) in the form of lipid droplets within hepatocytes as well as non-parenchymal liver cells, including Kupffer cells (KCs) [1]. Hepatic steatosis results from an imbalance between lipid uptake, synthesis, secretion and lipolysis, and is usually associated with dyslipidemia, insulin resistance, hypertension, type 2 diabetes and obesity [2]. The essential trigger for the transition of simple steatosis to NASH is not yet completely elucidated. Despite the high global prevalence of NAFLD (32.4%) in the general population [3], no FDA-approved medication is available yet for the treatment of NAFLD/NASH. In fact, lifestyle adjustment is still the main clinical intervention.

Inflammation contributes to the transition of simple steatosis to NASH and liver-resident KCs play a pivotal role in NAFLD/NASH pathogenesis [4]. Once activated during NAFLD progression, KCs produce pro-inflammatory factors, such as monocyte chemoattractant protein 1 (MCP-1) and tumor necrosis factor (TNF), leading to increased hepatic monocyte recruitment and inhibition of canonical insulin signaling, further aggravating liver injury and steatosis [5,6]. In addition, KC-derived pro-fibrinogenic factors increase collagen production by hepatic stellate cells, generating a vicious circle that exacerbates NAFLD and inflammation, and derive progression towards NASH [7,8]. Thereby, selective depletion of KCs from the liver alleviates hepatocellular damage and prevents diet-induced hepatic steatosis and insulin resistance [9,10]. Furthermore, consumption of a cholesterol-rich diet causes cholesterol accumulation in KCs to yield foamy inflammatory KCs, which directly contribute to liver inflammation [11]. Recently, we and others showed that NAFLD/NASH impaired KC self-renewal and induce KC death, thus reducing embryonically-derived liver-resident KCs [12-14]. This KC niche is replenished through recruitment, differentiation, and proliferation of monocyte-derived macrophages, which are however reported to be more inflammatory than KCs and to contribute to aggravation of liver inflammation and damage [12,13].

Liver X receptors (LXRs), *i.e*., the LXRα and LXRβ isoform, are essential (oxy)sterol-activated transcription factors involved in lipid metabolism and immune responses [15,16]. LXRα is abundantly expressed in liver, adipose tissue, and macrophages, while LXRβ is ubiquitously expressed [17]. In macrophages, LXRα directly promotes reverse cholesterol transport via up-regulating ATP binding cassette (ABC) A1 [18]. Thus, LXRα-deficiency impairs cholesterol efflux and is associated with increased atherosclerosis [19,20]. Simultaneously, LXRs exert anti-inflammatory effects in immune cells [21], suppress KC activation, and protect against hepatic injury [22]. In addition, LXRs promote formation of long chain polyunsaturated fatty acids

(PUFAs), *e.g.* eicosapentaenoic acid and docosahexaenoic acid, which have anti-inflammatory activities [23,24]. The simultaneous regulation of lipid metabolism and inflammation serves LXRs as a potential drug target for NAFLD/NASH treatment [15,16]. However, at present no selective LXR agonists exist for the clinical treatment of NAFLD/NASH. This is mainly due to unfavorable effects of pharmacological LXR activation on sterol regulatory element-binding proteins (SREBPs)-induced lipogenesis, resulting in elevated atherogenic low density lipoprotein (LDL) cholesterol and triglycerides. Therefore, rather than alleviating liver lipid levels, most synthetic LXR agonists actually cause hepatic steatosis and hypertriglyceridemia [25,26]. Moreover, some synthetic LXR agonists have been reported to cause neutropenia due to down-regulation of neutrophil production in bone marrow and stimulation of their clearance by macrophages within peripheral tissues [27]. Taken together, a successful drug candidate for the treatment of NASH through LXR activation, should be LXR selective, not induce sterol regulatory element-binding transcription factor 1 (*Srebf1*), and not cause neutropenia.

Previously, we showed that desmosterol increases LXR target genes while inhibiting SREBP target genes in macrophages [28,29]. In addition, we reported that synthetic SH42 inhibits Δ24-dehydrocholesterol reductase (DHCR24), an important enzyme intertwining the Bloch and Kandutsch-Russell pathways of distal cholesterol biosynthesis, and causes accumulation of desmosterol [30]. Accordingly, we have recently reported that inhibition of DHCR24 induces LXR activation through accumulation of desmosterol, promoting resolution of inflammation without affecting *Srebf1c* expression in macrophages [24,31]. Taken together, we hypothesized that inhibiting DHCR24 increases desmosterol levels and subsequently induces LXR activation in KCs, thereby suppressing inflammation, without inducing lipid synthesis via *Srebf1*. Using our publishedDHCR24 inhibitor SH42 [31], we aimed to investigate the potential therapeutic effects of DHCR24 inhibition on diet-induced NAFLD development in APOE*3-Leiden.CETP mice, a well-established humanized mouse model for the study of (cardio)metabolic diseases.

Materials and Methods

Animals and treatments

Hemizygous *APOE*3-Leiden* (*E3L*) mice were crossbred with homozygous human cholesteryl ester transfer protein (CETP) transgenic mice to generate heterozygous *E3L.CETP* mice on a C57BL/6J background [32]. Because of phenotypical heterogeneity of *E3L.CETP* mice, non-responder mice were identified by 4-hour fasting plasma lipid levels, i.e., total cholesterol levels < 2 mM and triglyceride levels < 2 mM, and excluded before high fat high cholesterol diet (HFCD) treatment [33]. LXRα-deficient mice (also on C57BL/6J background), generated by

Deltagen using gene-targeting methods as described [34], were kindly provided by Tularik (San Francisco, CA, US). Mice were group-housed in individually ventilated cages in standard conditions at room temperature (22°C) with 40 ± 5% relative humidity and a 12-h light/dark (7 am lights on; 7 pm lights off) cycle. Water and standard laboratory diet (801203, Special Diets Services, UK) were available *ad libitum*, unless indicated otherwise. This study was approved by the Animal Ethical Committee of Leiden University Medical Center, Leiden, The Netherlands (AVD1160020173305, PE.18.034.007) and the Animal Ethical Committee of University Groningen, Groningen, The Netherlands (PE.18.034.030, 173305-02-001). All animals received humane care according to the criteria outlined in the NIH "Guide for the Care and Use of Laboratory Animals". All animal procedures were performed conform the guidelines from Directive 2010/63/EU of the European Parliament on the protection of animals used for scientific purposes.

At the age of 10-12 weeks, male *E3L.CETP* mice and LXRα-deficient mice were fed a HFCD (Altromin, Germany) containing 60% (energy) fat and 1% (wt/wt) cholesterol, and were randomized into two groups treated with either the DHCR24 inhibitor SH42 (0.5 mg·mouse^{-1}) [24,31] or vehicle (saline containing 3.3% ethanol and 3.3% Cremophor EL) 3 times per week by intraperitoneal injection. *E3L.CETP* mice were treated for 4 weeks (n= 6 mice per group) and 8 weeks (n= 8 mice per group) to evaluate effects on hepatic immune cells via flow cytometry analysis and hepatic steatosis via quantitative lipidomic analysis, respectively. LXRα-deficient mice were treated with either SH42 (n= 11 mice) or vehicle (n= 10 mice) for 4 weeks to evaluate effects on hepatic steatosis and immune cells. In a rescue experiment, male *E3L.CETP* mice were fed with HFCD for 10 weeks first and cotreated with SH42 (0.5 mg·mouse^{-1}) or vehicle (saline containing 3.3% ethanol and 3.3% Cremophor EL) 3 times per week by intraperitoneal injection for additional 8 weeks.

Body weight was measured weekly. Body composition (*i.e.* fat body and lean body mass; EchoMRI-100; EchoMRI, Houston, TX, USA) was evaluated before and after intervention. Food intake was determined during the treatment period.

Plasma glucose, insulin, and ALT assay

Four hour-fasted (9 am till 1 pm) blood samples were collected via tail vein of *E3L.CETP* mice bleeding into heparin-coated capillaries after 8 weeks treatment with vehicle or SH42. Blood samples were then centrifuged at 15,000g for 5 min at 4°C to collect plasma. 2.5 µL plasma was used to measure glucose (INstruchemie, The Netherlands) and 10 µL to measure insulin (Mercodia AB, Sweden) according to the manufacturers' protocols. The homeostatic Model Assessment for Insulin Resistance (HOMA-IR) scores were calculated using the equation: HOMA-IR= fasting insulin (mU·L^{-1}) × fasting glucose (mmol·L^{-1})/22.5 [35].

To measure ALT levels, 4 hour-fasted (9 am till 1 pm) blood samples were collected via tail vein of *E3L.CETP* mice after 16 weeks of HFCD treatment. Blood samples were then

centrifuged at 15,000g for 5 min at 4°C to collect plasma. Two µL plasma was diluted 200 times and used for plasma ALT assay (ab282882, Abcam, UK) according to the manufacturer's protocol.

Liver histology and hepatic steatosis scoring

After 8 or 18 weeks of treatment in *E3L.CETP* mice or 4 weeks in LXRα-deficient mice, mice were killed and transcardially perfused with ice-cold PBS, and a small piece of the right liver lobe was collected and fixed in phosphate-buffered 4% formaldehyde. Fixed tissues were embedded in paraffin and cut into sections of 5 µm thickness for staining with hematoxylin and eosin (HE) and/or the macrophage marker F4/80 (1 $\mu g \cdot mL^{-1}$, MCA497, Serotec, Oxford, UK) which was detected using ImmPRESS HRP goat anti-rat IgG detection kit (MP-744-15, Vector Laboratories, CA, USA). Hepatic steatosis was evaluated from HE stained slides by two blinded experts respectively, with the criteria proposed by Liang *et al* [36]. Hepatocellular vesicular steatosis, *i.e.* microvesicular steatosis and macrovesicular steatosis, and hepatocellular hypertrophy were scored (grade 0 - 3) based on the percentage of the total area affected, and the grades were summed into one standard as "steatosis score" (0 - 9). Liver Oil Red O staining was performed on frozen liver tissue sections to visualize and quantify lipid droplets using ImageJ software (version 1.50i). F4/80 positive area using F4/80 stained slides were quantified using ImageJ software (version 1.50i). Hepatic crown-like structures formed by macrophages aggregating around dead hepatocytes were counted from F4/80 stained slides which were blinded before analysis and expressed as number per area [37]. To quantify the collagen content, liver sections were stained with Sirius red/Fast green and quantified using ImageJ software (version 1.50i). Values in figures for each staining present means of 9 randomly selected image fields (0.468 mm^2 per field) per mouse. The antibody used is listed in **Appendix Table S1**.

GC-MS analysis of desmosterol

After 8 weeks of treatment in *E3L.CETP* mice or 4 weeks in LXRα-deficient mice, desmosterol levels were measured using GC-MS after alkaline hydrolysis, as described previously for plasma [31] and liver [24]. In brief, a Bruker Scion GC-MS system (used for *E3L.CETP* mice) or an Agilent 7890B coupled to a 5977B MS (used for LXR KO mice) were utilized and operated in selected ion monitoring mode (SIM). An Agilent VF-5ms column, 25 m × 0.25 mm × 0.25 µm was used. Helium 99.9990% was used as carrier gas at a constant flow rate of 1.4 mL per min. Injector and transfer line were operated at 280°C. The oven program started at 90°C held for 0.5 min, then ramped to 270°C at 30°C per min, and ramped to 310°C at 10°C per min. The following masses were used to quantify desmosterol levels against an external calibration line (0 - 10 ppm) *m/z* 445 + 355 for cholestanol (IS), *m/z* 357 and 271 for cholestan (IS) and *m/z* 343 + 253 or 441.2 for desmosterol. Desmosterol was identified by matching characteristic ions and retention times with an authentic standard (Sigma Aldrich).

Quantitative lipidomic analysis

Quantitative lipidomic analysis was carried out in liver and plasma samples in *E3L.CETP* mice and in LXRα-deficient mice as described elsewhere [24]. Briefly, a small piece of the right liver lobe was homogenized with 600 µL LCMS grade water in a bullet blender for 30 sec and an aliquot corresponding to 5 mg liver tissue was used. For plasma samples, 25 µL was used. 25 µL internal standard mix (100 µL for liver samples) (Lipidyzer™ internal standard kit, containing > 50 labelled internal standards for 13 lipid classes, Sciex cat# 504156), 500 µL methyl tert-butyl ether (MTBE), and 160 µL methanol were subsequently added and the mixture was shaken for 30 min at room temperature. After adding 200 µL water, samples were centrifuged at 16,000 g for 3 min and the upper organic layer was collected in a glass vial. The remaining sample was extracted again by adding 300 µL MTBE, 100 µL methanol and 100 µL water for 30 min. The organic extracts were then pooled and dried under a gentle stream of nitrogen. The dry extract was subsequently dissolved in 250 µL Lipidyzer running buffer and analysed according to the manufacturer's protocol. For data analysis, 13 lipid classes, including cholesteryl esters (CE), ceramides (CER), diacylglycerols (DAG), dihydroceramides (DCER), free fatty acids (FFA), hexosylceramides (HCER), lysophosphatidylcholines (LPC), lysophosphatidylethanolamines (LPE), phosphatidylcholines (PC), phosphatidylethanolamines (PE), sphingomyelins (SM) and triacylglycerols (TAG) were compared.

Isolation of liver immune cells and peripheral blood mononuclear cells

After 4 weeks of SH42 treatment, blood and liver was collected and processed for flow cytometry as described previously [38]. In short, blood was collected from the retro-orbital sinus of anesthetized mice into heparin capillaries, after which mice were killed and transcardially perfused with PBS for 5 min to remove circulating cells. A piece of right liver lobe was cut off for other liver assays and the remainder liver tissues were minced with a scalpel to form a paste, digested with collagenase type IV (Sigma Aldrich, US), and hepatocytes were removed by low gravity centrifugation at 50 g for 3 min. $CD45^+$ leukocytes were isolated using CD45 microbeads (35 µL beads per liver; Miltenyi Biotec, US) and an LS column, according to the manufacturer's instructions. In addition, peripheral blood mononuclear cells were isolated. To this end, 450 µL blood was mixed with red blood cell lysis/fix buffer (Becton Dickinson, US) (3:20; v/v) for 15 min at room temperature. Subsequently, white blood cells were pelleted by centrifugation at 600 g for 5 min. The supernatant was discarded and cells were resuspended and washed with PBS. The cells isolated from the liver and blood were counted and characterized by flow cytometry.

Flow cytometry analysis

All cell suspensions were stained with the fixable viability dye Zombie-UV (BioLegend, US) and fixed with 1.9% paraformaldehyde. Within 24 h of fixation, the cells were pre-incubated

with an Fcγ blocking antibody (Thermo Fisher Scientific) for 15 min. The cells were then stained with fluorescently labelled antibodies listed inthe Appendix Table S2 for 30 min at 4℃ in the dark. Fluorescently labelled cells were measured on an LSRII (Becton Dickinson) and gates were set according to Fluorescence Minus One (FMO) controls using FlowJoTM Software (Becton Dickinson). Representative gating schemes are shown in Appendix Fig. S3 **and S4**.

Statistical analysis

Group size was determined by power analysis of data from our previous studies to achieve statistical power of 80% and p value of 0.05. Mice were randomized into different groups before the treatments. Investigators were blinded for hepatic steatosis scoring and were not blinded for other assays. Outliers were identified using Grubbs' test (https://www.graphpad.com/quickcalcs/Grubbs1.cfm) and removed from statistical analysis, which is clearly stated in figure legends if applicable. Because some datasets did not pass a statistical test for Gaussian distribution, differences between two groups were compared using a non-parametric Mann-Whitney test performed in GraphPad Prism 8.1 (GraphPad Software). For quantification of different lipid classes, Benjamini-Hochberg correction was used for multiple hypothesis testing (Figure 1G-1J and 4E-4H). $p<0.05$ was considered significant (*$p<0.05$, **$p<0.01$, ***$p<0.001$).

Results

Inhibition of DHCR24 by SH42 markedly increases liver desmosterol levels and ameliorates hepatic steatosis

To assess the effects of DHCR24 inhibition on hepatic steatosis, *E3L.CETP* mice were fed a HFCD while being treated with vehicle or the synthetic DCHR24 inhibitor SH42 [24,31] for a period of 8 weeks (**Fig. EV1A**). SH42 treatment did not affect food intake (**Fig. EV1B**), while temporarily preventing HFCD-induced body weight gain as compared to control group (**Fig. EV1C**). After 8 weeks of treatment, body weight and body composition, *i.e*., lean body mass (**Figure EV1D**) and fat body mass (**Figure EV1E**) of SH42 treated mice was comparable to that of the control group. In addition, the weight of various tissues (*i.e.,* liver, white adipose tissue, kidney, heart, lung, spleen, and brown adipose tissue) was unchanged by SH42 treatment (**Fig. EV1F**). As anticipated, SH42 markedly increased hepatic desmosterol levels (10-fold, **Fig. 1A, Fig. EV1G**).

Hepatic steatosis was evaluated by HE staining and scored as described previously [36]. As compared to the control treatment, SH42 treatment ameliorated diet-induced hepatic steatosis (**Fig. 1B**), as evident by a clear reduction of the hepatic steatosis score (-58%, **Fig.**

1C), and liver lipid area stained by Oil Red O (-53%, **Fig. 1B and D**). We next analysed liver lipid profiles by comprehensive lipidomic analysis. Firstly, we observed a clear alteration in the lipid class composition after SH42 treatment (**Fig. 1E**). Specifically, SH42 treatment caused a relative reduction of TAG (-21%) and DAG (-22%), accompanied by a relative increase of the other lipid classes, including CER, PC, PE, and SM (**Fig. 1E, Appendix Fig. S1**). Volcano plot analysis of the lipid species concentrations of different lipidomes revealed the majority of significantly altered lipid species by SH42 treatment were down-regulated, and most of them were TAGs (**Fig. 1F**). Consistently, SH42 tended to decrease hepatic concentrations of triacylglycerides (TAG) (-39%; p=0.06, p_adj=0.08, **Fig. 1G**) and diacylglycerides (DAG) (-20%; p=0.08, p_adj=0.08, **Fig. 1H**). In addition, SH42 treatment reduced hepatic free fatty acids (FFA) (-16%; p=0.02, p_adj=0.08, **Fig. 1I**) and cholesterol ester (CE) levels (-25%; p=0.08, p_adj=0.08, **Fig. 1J**). Despite these strong effects on hepatic lipid content, SH42 did not affect fasting plasma glucose, insulin, or homeostatic Model Assessment for Insulin Resistance (HOMA-IR) scores (**Fig. EV1H-J**). Taken together, inhibition of DHCR24 by SH42 markedly increases liver desmosterol levels, accompanied by amelioration of diet-induced hepatic steatosis without marked effects on body composition and glucose homeostasis.

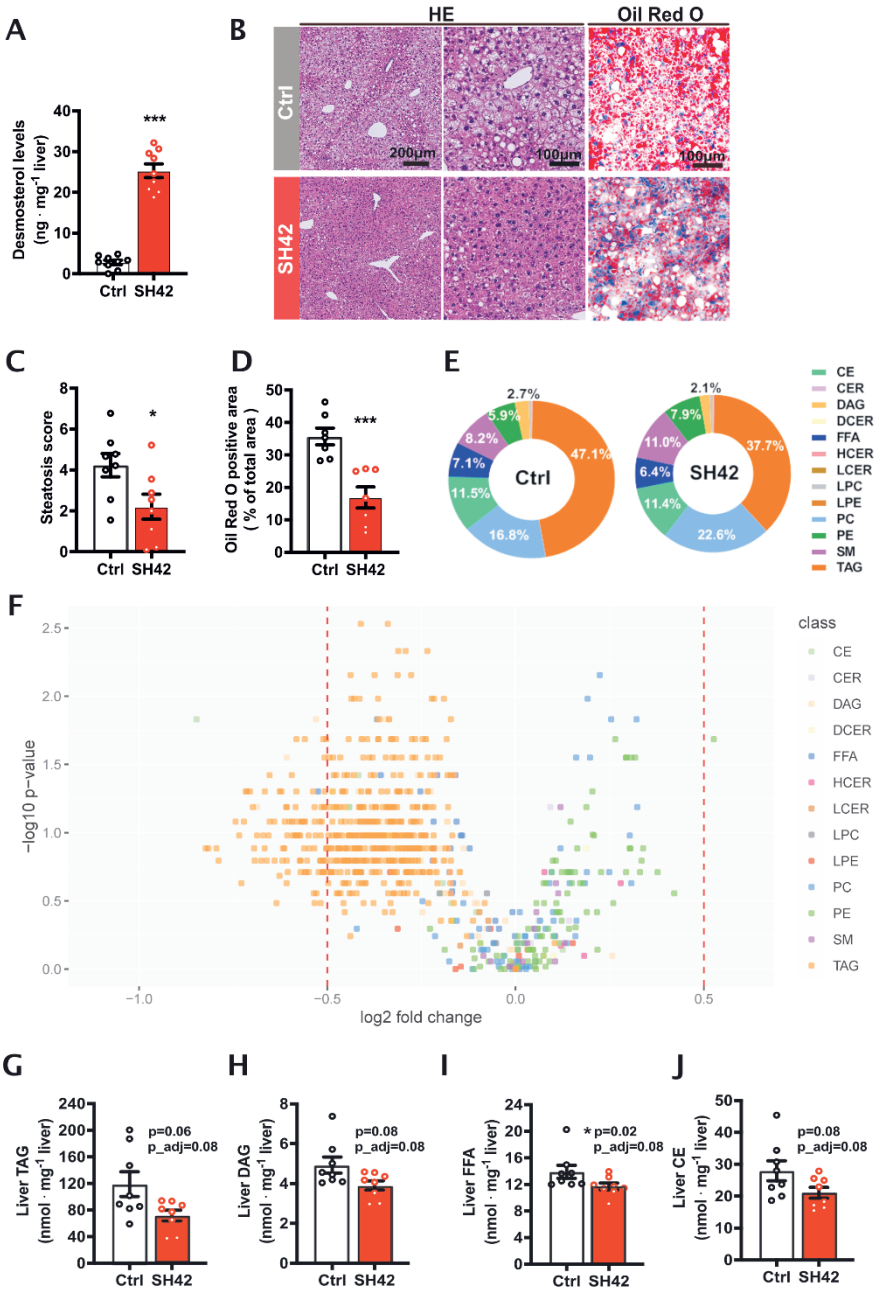

Fig. 1. Inhibition of DHCR24 by SH42 markedly increases liver desmosterol and ameliorates hepatic steatosis. *E3L.CETP* mice fed a high fat high cholesterol diet (HFCD) were treated with vehicle (Ctrl) or DHCR24 inhibitor SH42 (SH42) (n= 8 mice per group). (**A**) After 8 weeks of treatment, mice were sacrificed and livers were collected to measure desmosterol levels, and (**B**) to stain with haematoxylin and eosin (HE) and Oil Red O. (**C**) Hepatic steatosis was scored using the HE stained slides and (**D**) lipid

positive area was quantified using the Oil Red O stained slides (n= 7 mice per group; two values were identified as outliers based on Grubbs' test and removed from statistical analysis). (**E**) Liver lipid classes were analysed (**Appendix Fig S1**), and the relative average abundance of lipid classes in each group are depicted as pie charts. (**F**) Volcano plot analysis of liver lipid species concentrations is shown. Hepatic (**G**) TAG, (**H**) DAG, (**I**) FFA and (**J**) CE lipid class concentrations were summarized. Benjamini-Hochberg correction was used for multiple hypothesis testing and Benjamini Hochberg adjusted p-values are presented (p_adj). Data information: Values are mean ± SEM. Differences between two groups (SH42/Ctrl) were determined using a Mann-Whitney test. *p<0.05, ***p<0.001 vs. control (ctrl). Abbreviations: CE, cholesteryl esters; CER, ceramides; DAG, diacylglycerols; DCER, dihydroceramides; FFA, free fatty acids; HCER, hexosylceramides; LPC, lysophosphatidylcholines; LPE, lysophosphatidylethanolamines; PC, phosphatidylcholines; PE, phosphatidylethanolamines; SM, sphingomyelins; TAG, triacylglycerols. Scale bar: 100 µm or 200 µm as indicated**.**

Inhibition of DHCR24 by SH42 prevents Kupffer cell activation and reduces immune cell infiltration into the liver

We next evaluated the effect of DHCR24 inhibition on the hepatic inflammation in mice treated with SH42 or vehicle for 8 weeks by immunohistochemistry. SH42 treatment significantly reduced the hepatic F4/80 content (-29%, **Fig. 2A, B**) as well as the number of hepatic crown-like structures of macrophages surrounding dying hepatocytes (-79%, **Fig. 2C**), which is a prominent feature of NASH development [37].

Flow cytometry on MACS-purified hepatic leukocytes revealed that 4 weeks SH42 treatment tended to decrease total hepatic leukocytes (-37%; p=0.09, **Fig. 2D**). Given the critical role of KCs in the progression of NASH [9,10], we next explored the effects of DHCR24 inhibition on KCs. We observed a significant increase in total KCs upon SH42 treatment (+44%, **Fig. 2E, F**). Although SH42 did not significantly reduce $MHCII^+/CD11c^+$ activated KCs (**Fig. 2G, H**), $MHCII^-/CD11c^-$ resting KCs were significantly increased (+21%, **Fig. 2G, I**), indicative of prevented KC activation. In addition, SH42 treatment reduced monocytes in both liver (-79%, **Fig. 2J**) and blood (-43%; p=0.06, **Fig. EV2A, B**), and decreased hepatic neutrophils (-50%, **Fig. 2K**) without affecting circulating neutrophils (**Fig. EV2A, C**). Together, these data indicate that SH42 treatment prevents KC activation, limits hepatic immune cell recruitment and dampens hepatic inflammation.

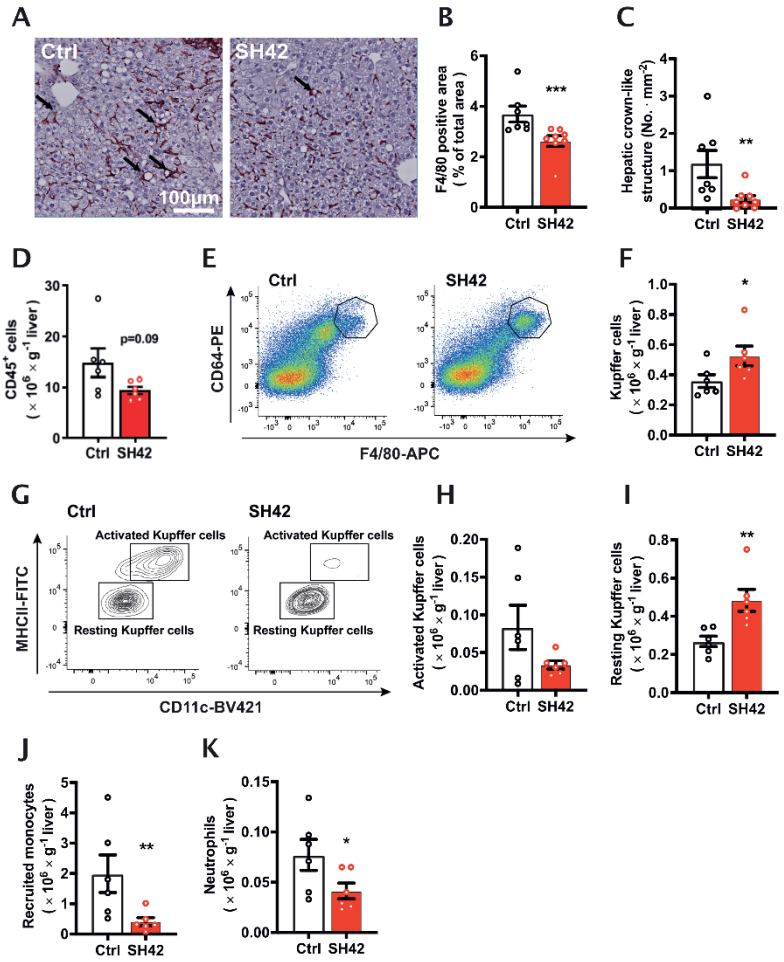

Fig. 2. Inhibition of DHCR24 by SH42 prevents Kupffer cell activation and reduces immune cell infiltration into the liver. E3L.CETP mice fed a HFCD were treated with vehicle (Ctrl) or DHCR24 inhibitor SH42 (SH42) (n= 8 mice per group). After 8 weeks of treatment, mice were killed and livers were collected to stain with F4/80. (**A**) Representative pictures of F4/80 staining are shown and (**B**) F4/80 positive area was quantified. (**C**) Hepatic crown-like structures as indicated by the arrows in Fig. 2A were counted (n= 7 and 8 mice, respectively; one value was identified as an outlier based on a Grubbs' test and removed from statistical analysis). In another experiment after 4 weeks of treatment (n= 6 mice per group), fresh livers were collected to isolate and count (**D**) CD45+ cells. (**E**, **F**) Total Kupffer cells (KCs), (**G**, **H**) activated KCs, (**G**, **I**) resting KCs, (**J**) recruited monocytes, and (**K**) neutrophils in the liver were measured via flow cytometry. Data information: Values are mean ± SEM. Differences between two groups (SH42/Ctrl) were determined using a Mann-Whitney test. *p<0.05, **p<0.01, ***p<0.001vs. ctrl. Scale bar: 100 µm.

Inhibition of DHCR24 by SH42 does not increase circulating lipids

Consistent with the potent increase in hepatic desmosterol levels, SH42 also markedly increased plasma desmosterol levels from undetectable levels (< 0.5 µg·mL^{-1}) to 3.1 ± 0.4 µg·mL^{-1} (**Fig. 3A**). Since synthetic LXR agonists usually induce lipogenesis and hypertriglyceridemia as unwanted effects [25,27], we next determined the effect of 8 weeks of SH42 treatment on circulating lipid levels using quantitative comprehensive lipidomic analysis. Analysis of the plasma lipidome revealed that SH42 treatment relatively decreased circulating CE while relatively increasing lactosylceramides (LCER), phosphatidylcholine (PC) and phosphatidylethanolamine (PE) (**Appendix Fig. S2**). With respect to absolute lipid concentrations, SH42 did not affect plasma levels of total TAG (**Fig. 3B**) and DAG (**Fig. 3C**), while significantly decreasing plasma levels of FFA (-16%, **Fig. 3D**) and CE (-24%; p=0.08, **Fig. 3E**). These data imply that inhibition of DHCR24 by SH42 increases plasma desmosterol levels and decreases FFA and CE levels, importantly without inducing hypertriglyceridemia.

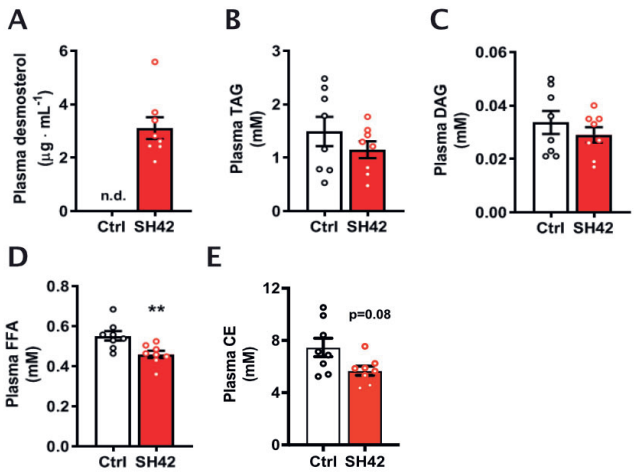

Fig. 3. Inhibition of DHCR24 by SH42 does not increase circulating lipids. *E3L.CETP* mice fed a HFCD were treated with vehicle (Ctrl) or DHCR24 inhibitor SH42 (SH42) (n= 8 mice per group). (**A**) After 8 weeks of treatment, blood was collected to measure desmosterol levels and for quantitative lipidomic analysis. Plasma (**B**) TAG, (**C**) DAG, (**D**) FFA and (**E**) CE lipid class concentrations were summarized. Data information: Values are mean ± SEM. Differences between two groups (SH42/Ctrl) were determined using a Mann-Whitney test. **p<0.01 vs. ctrl. Abbreviations: CE, cholesteryl esters; DAG, diacylglycerols; FFA, free fatty acids; TAG, triacylglycerols.

The therapeutic effects of DHCR24 inhibition by SH42 on hepatic steatosis are strictly dependent on LXRα

Based on previous reports [24,28,29], we hypothesized that the therapeutic effects of SH42 were attributed to LXR activation triggered by increased desmosterol levels as a result of DHCR24

inhibition. Since LXRα plays a crucial role in both lipid metabolism [39] and macrophage/KC homeostasis [19,20,40], we next evaluated the effects of 4 weeks of SH42 treatment in HFCD-fed LXRα-deficient mice to evaluate the importance of LXRα in the observed protective effects of SH42 in ameliorating hepatic steatosis and inflammation. SH42 treatment had no effect on body weight (**Fig. EV3A**), body composition (**Fig. EV3B, C**) or liver weight (**Fig. EV3D**) in LXRα-deficient mice. Consistent with previous findings that LXRα-deficient mice are more susceptible to high fat diet-induced hepatic steatosis and inflammation [40,41], we observed significant hepatic steatosis after 4 weeks of HFCD (**Fig. 4A, B**). Although SH42 treatment largely increased plasma desmosterol levels also in LXRα-deficient mice (+80%, **Fig. EV3E**), it failed to improve hepatic steatosis (**Fig. 4A**) as evidenced by an unchanged steatosis score (**Fig. 4B**) and similar lipid positive areas stained by Oil Red O in SH42 treated mice compared to control (**Fig. 4A, C**). Liver lipidomic analysis further revealed that almost no lipid species was significantly changed upon SH42 treatment as shown by volcano plot analysis (**Fig. 4D**). Accordingly, SH42 treatment showed no effects on hepatic concentrations of TAG (**Fig. 4E**), DAG (**Fig. 4F**), FFA (**Fig. 4G**) or CE (**Fig. 4H**) in absence of LXRα.

>> Fig. 4. The therapeutic effects of DHCR24 inhibition on hepatic steatosis are strictly dependent on LXRα. LXRα deficient mice fed HFCD were treated with vehicle (Ctrl) or DHCR24 inhibitor SH42 (SH42) . (n= 10 and 11 mice, respectively). (**A**) After 4 weeks of treatment, mice were killed and liver samples were collected to stain with HE and Oil Red O. (**B**) Hepatic steatosis was scored using the HE stained slides and (**C**) lipid positive area was quantified using the Oil Red O stained slides. (**D**) Volcano plot analysis of liver lipid species concentrations is shown. Hepatic (**E**) TAG, (**F**) DAG, (**G**) FFA and (**H**) CE lipid class concentrations were summarized. Benjamini-Hochberg correction was used for multiple hypothesis testing and Benjamini Hochberg adjusted p-values are presented (p_adj). One outlier was identified and excluded in the hepatic CE analysis. Data information: Values are mean ± SEM. Differences between two groups (SH42/Ctrl) were determined using a Mann-Whitney test if not indicated otherwise. Scale bar: 100 µm or 200 µm as indicated. Abbreviations: CE, cholesteryl esters; CER, ceramides; DAG, diacylglycerols; DCER, dihydroceramides; FFA, free fatty acids; HCER, hexosylceramides; LPC, lysophosphatidylcholines; LPE, lysophosphatidylethanolamines; PC, phosphatidylcholines; PE, phosphatidylethanolamines; SM, sphingomyelins; TAG, triacylglycerols.

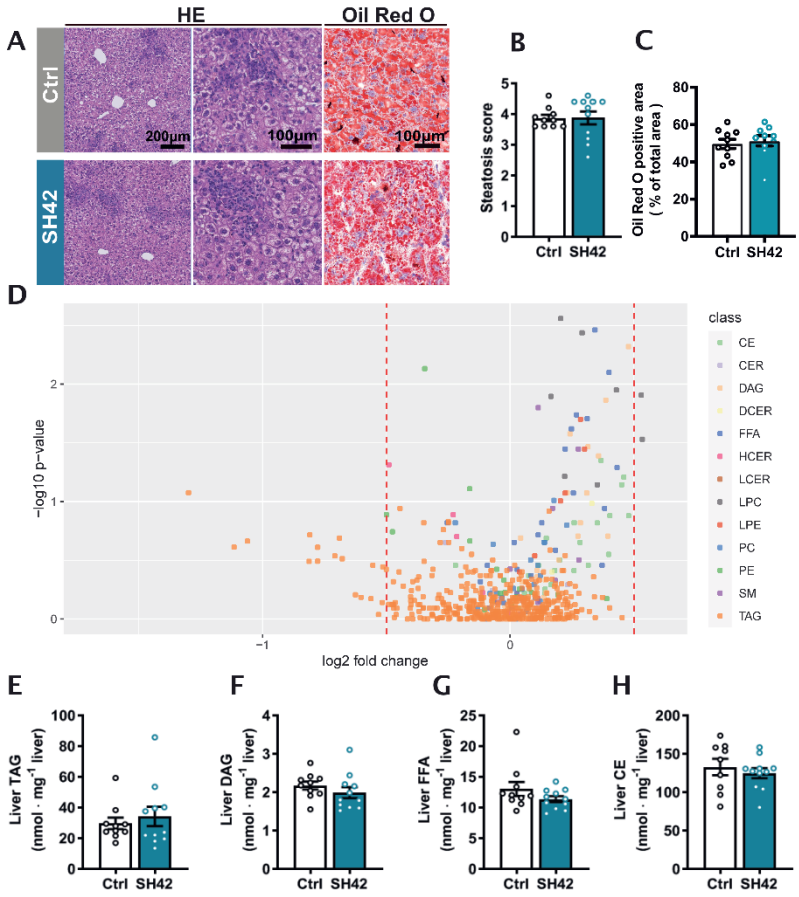

The therapeutic effects of DHCR24 inhibition by SH42 on Kupffer cell activation and hepatic monocyte infiltration are strictly dependent on LXRα

Subsequently, we analysed hepatic immune cells by flow cytometry after 4 weeks treatment with SH42 in HFCD-fed LXRα-deficient mice. In contrast to *E3L.CETP* mice, SH42 did not affect hepatic leukocytes (**Fig. 5A**) in LXRα deficient mice. Strikingly, SH42 did not affect KC numbers (**Fig. 5B, C**), and did not prevent KC activation as evidenced by unchanged high levels of NASH-associated $MHCII^{+}CD11c^{+}$ activated KCs (**Fig. 5D, E**) and $MHCII^{-}CD11c^{-}$ resting KCs (**Fig. 5D, F**). SH42 did not reduce recruited monocytes in liver (**Fig. 5G**) but reduced hepatic neutrophils in LXRα-deficient mice (-42%; **Fig. 5H**). Congruent with these data, circulating monocytes and neutrophils were not affected by SH42 treatment (**Fig. EV4A-C**). Taken together, these data show that inhibition of DHCR24 by SH42 does not prevent diet-induced hepatic steatosis and inflammation in LXRα deficient mice.

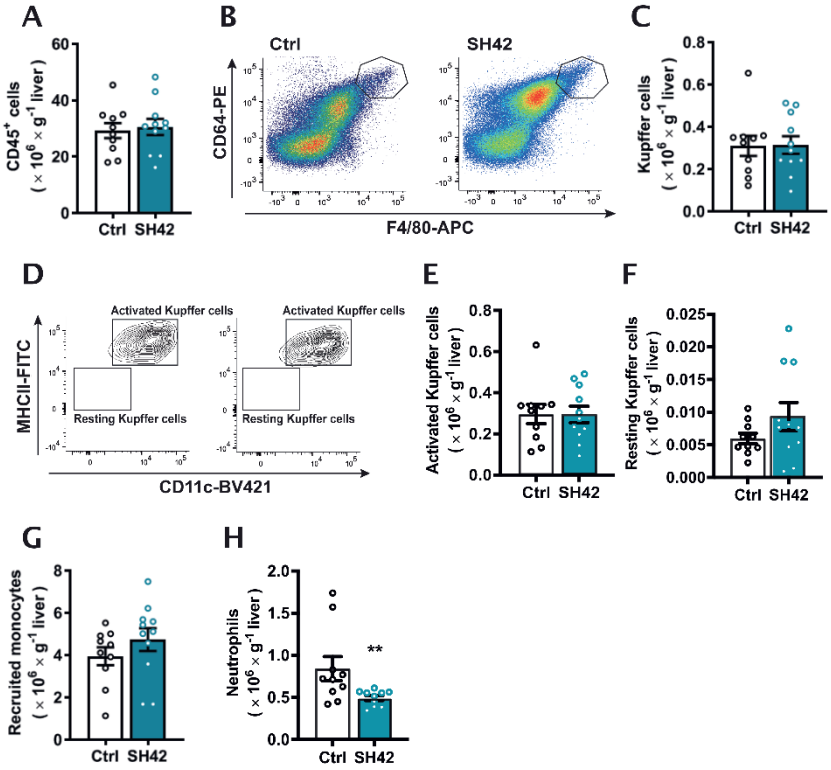

Fig. 5. The therapeutic effects of DHCR24 inhibition on liver inflammation are strictly dependent on LXRα. LXRα deficient mice fed HFCD were treated with vehicle (Ctrl) or DHCR24 inhibitor SH42 (SH42) (n= 10 and 11 mice, respectively). (**A**) After 4 weeks of treatment, mice were killed and fresh liver samples were collected to isolate and count $CD45^+$ cells. (**B**, **C**) Total Kupffer cells (KCs), (**D**, **E**) activated KCs, (**D**, **F**) resting KCs, (**G**) recruited monocytes, and (**H**) neutrophils in the liver were measured via flow cytometry. Data information: Values are mean ± SEM. Differences between two groups (SH42/Ctrl) were determined using a Mann-Whitney test. **p<0.01 vs. ctrl.

Treatment with SH42 reduces hepatic crown-like structures, liver collagen content, and plasma alanine transaminase levels in an established NAFLD model

Translationally, we next investigated if inhibition of DHCR24 could rescue NASH progression. To this end, *E3L.CETP* mice were fed with a HFCD for 10 weeks first to establish NAFLD, and then treated with vehicle or SH42 while still on HFCD for an additional 8 weeks (**Fig. 6A**). SH42 treatment did not significantly influence either total body weight (Fig. S7A) or composition (**Fig. EV5A-C**). Although we did not observe any difference in liver weight (**Fig. EV5D**) and hepatic steatosis (**Fig. 6B-D**), SH42 treatment reduced hepatic crown-like structures (-89%; **Fig. 6E, F**) without significant influence on the F4/80 positive area (**Fig. 6E, G**), and ameliorated liver collagen content (-50%; **Fig. 6H, I**). In addition, SH42 treatment reduced plasma levels of the liver injury marker plasma alanine transaminase (ALT) (-42%;

Fig. 6J). These effects were accompanied with a robust increase in plasma desmosterol levels (>400-fold; **Fig. EV5E**).

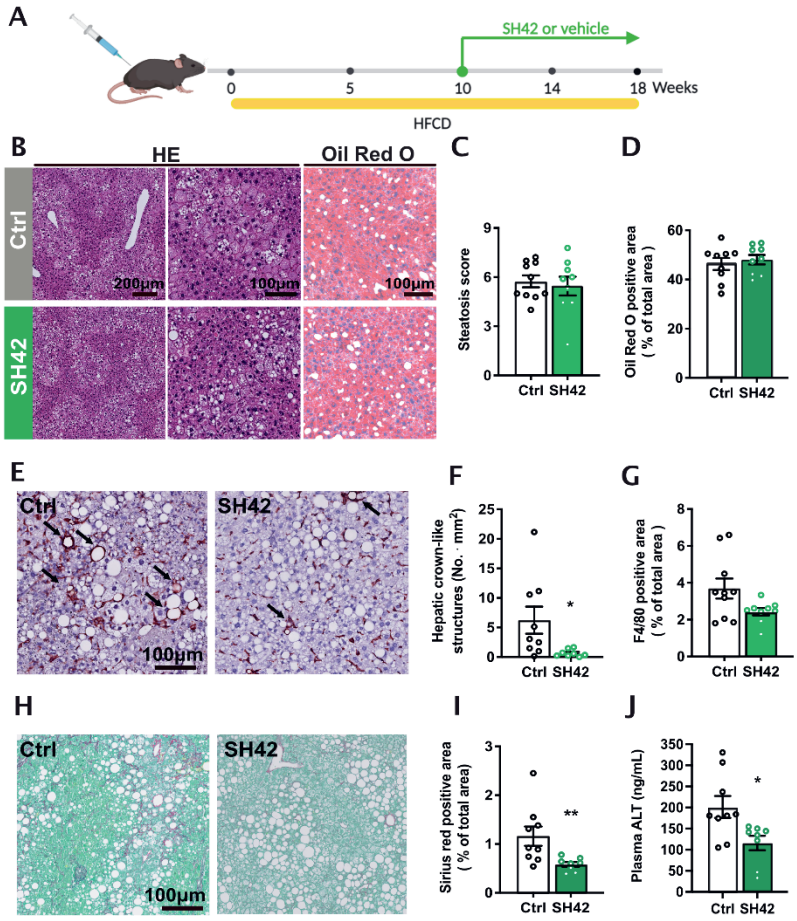

Fig. 6. Treatment with SH42 reduces hepatic crown-like structures, liver collagen content, and plasma alanine transaminase levels in an established NAFLD model. (**A**) *E3L.CETP* mice were fed with a HFCD for 10 weeks first and then treated with vehicle (Ctrl) or DHCR24 inhibitor SH42 (SH42) (n= 10 and 9 mice, respectively) for additional 8 weeks. Mice were killed and livers were collected. (**B**) Liver sections were stained with haematoxylin and eosin (HE) and Oil Red O. (**C**) Hepatic steatosis was scored using the HE stained slides and (**D**) lipid positive area was quantified using the Oil Red O stained slides. Liver sections were stained with F4/80 (**E**) to quantify (**F**) hepatic crown-like structures as indicated by the arrows in Fig. 6E and (**G**) F4/80 positive area. To quantify the collagen content, liver sections were stained with (**H**) Sirius red/Fast green and (**I**) quantified accordingly. (**J**) Blood samples were collected after 18 weeks treatment and plasma alanine transaminase (ATL) levels were measured. Data information: Values are mean ± SEM. Differences between groups (SH42/Ctrl) were determined using a Mann-Whitney test. *p<0.05, **p<0.01, vs. ctrl. Scale bar: 100 µm or 200 µm as indicated.

Discussion

As key regulators of metabolic and inflammatory signaling [15,16], LXRs have taken center stage as potential therapeutic targets for the treatment of cardiometabolic diseases. However, undesirable side effects of pharmacological LXR activation, including hyperlipidemia via induction of *Srebf1c* expression and neutropenia [25,27], have prevented clinical application. Interestingly, desmosterol has been reported to be an endogenous ligand of LXR while inhibiting SREBP activity [29]. Therefore, enhancing endogenous desmosterol levels by targeting DHCR24 is already considered as a promising strategy for activating LXR transcription programs to combat atherosclerotic cardiovascular disease [28,29,42]. In this study, we exploited the synthetic DHCR24 inhibitor SH42, developed by our group [31], for the treatment of hepatic steatosis and inflammation, *i.e.*, the two hallmarks of NAFLD/NASH development. We show that inhibition of DHCR24 induces marked increases in desmosterol levels in both liver and circulation which is accompanied by decreased hepatic steatosis and inflammation. Experiments performed in LXRα-deficient mice demonstrated that the therapeutic effects of SH42 are strictly dependent on LXRα activation, most likely due to increased desmosterol, as we have previously shown that SH42 does not have intrinsic LXR affinity [24].

We found that inhibition of DHCR24 by SH42 markedly increased desmosterol levels in both *E3L.CETP* mice and LXRα-deficient mice, while SH42 prevented circulating monocyte recruitment and increased $MHCII^-/CD11c^-$ resting KCs in *E3L.CETP* mice only (**Fig. 2G-J**). This effect on monocytes/KCs is likely attributed to the direct effects of desmosterol-induced LXRα activation in monocytes/KCs, based on our previous study showing that desmosterol activates LXR in macrophages but not in hepatocytes [29,43]. In addition, we previously showed that inhibition of DHCR24 by SH42 increased desmosterol and induced the expression of LXR target genes, including *Abca1* and *Abcg1* in RAW 264.7 macrophages [24]. LXRα is highly expressed in KCs and the region of enhancers unique to KCs are enriched in LXR-regulating sequence motifs [44], indicating a role of LXRs in KC homeostasis. Accordingly, we here observed that about 95% of KCs in LXRα-deficient mice displayed markers indicative of activated KCs (*i.e*. $MHCII^+/CD11c^+$ KCs) versus less than 25% of KCs in wild type mice upon feeding the same HFCD, which is in agreement with our previous study in LXRα-deficient mice showing a robust increase in KC activation and hepatic inflammation [40]. Taken together, our study suggests that pharmacological inhibition of DHCR24 is a feasible way to prevent KC activation and alleviate liver inflammation through desmosterol-induced LXRα activation.

Importantly, we observed that inhibition of DHCR24 by SH42 prevented high fat diet-induced hepatic steatosis in *E3L.CETP* mice (**Fig. 1**) but not in LXRα-deficient mice (**Fig. 4**). We excluded the potential contribution of altered systemic glucose homeostasis in this process as evidenced by unchanged body composition, circulating glucose and insulin levels, as well

as HOMA-IR scores in both groups (**Fig. EV1**). We reasoned that the alleviated liver inflammation may largely contribute to the reduction of hepatic steatosis. The feed-forward loop between lipotoxic hepatocytes and proinflammatory immune cells, especially KCs, promotes NAFLD/NASH progression [45]. Our study strongly suggests that this vicious circle can be abrogated by desmosterol-induced LXRα activation in liver-resident KCs. Consistently, both prevention of KC activation and depletion of KCs reduces liver inflammation [46] and alleviates hepatic steatosis [9,10]. Therefore, the alleviated liver inflammation could be the direct effect of desmosterol in macrophages/KCs, which subsequently prevents hepatic steatosis. Additional, alleviation of liver inflammation has been shown to have multiple effects, including reduced fatty acid uptake, VLDL secretion, and lipid oxidation [47], which could be the cause of a reduction in liver lipids by SH42 treatment, and needs to be further investigated.

Pharmaceutical development of LXR agonists has been challenged by the fact that these compounds usually induce *de novo* lipogenesis [25,27], which is mainly attributable to hepatocyte-specific LXRα activation [48,49]. Importantly, DHCR24 inhibition by SH42 decreases plasma FFA and CE levels, without increasing plasma total TAG and DAG levels (**Fig. 3**), which implies that LXRα activation by desmosterol, in contrast to synthetic agonists, does not lead to hyperlipidemia. This can be easily understood from the fact that desmosterol activates LXRα in macrophages/KCs only, whereas LXR-induced hyperlipidemia is mainly due to increased *de novo* lipogenesis within hepatocytes [29]. In fact, we have shown that desmosterol even suppresses SREBPs in macrophages via an Insig/SREBP cleavage-activating protein (SCAP)-dependent mechanism [28,29,42]. Taken together, SH42-induced desmosterol does not evoke an undesirable increase in plasma and hepatic lipid levels that are typical for synthetic LXR agonists, likely by selective LXRα activation in macrophages/KC rather than hepatocytes.

A human study has demonstrated that desmosterol levels in circulation and liver are associated with NASH development [50]. However, whether desmosterol has a specific role in the pathophysiology of NAFLD/NASH is still unknown. To the best of our knowledge, our present study for the first time shows the potential application of pharmacological DHCR24 inhibition to enhance endogenous desmosterol levels for the treatment of NAFLD/NASH. Interestingly, a recent genetic study demonstrated that the rs588709 variant near the *DHCR24* locus is associated with lower circulating TAG-rich VLDL particles [51], which potentially extends the role of DHCR24 to human lipid metabolism. Triparanol is the most widely used (nonspecific) DHCR24 inhibitor [52]; however, it was withdrawn from clinical application due to severe adverse side effects, such as nausea and vomiting, cataracts, and skin disorders [53]. In contrast to Triparanol with an IC_{50} value of 14 μM, SH42 is a much more potent DHCR24 inhibitor, having an IC_{50} value of less than 10 nM in a cellular assay [31,54] as judged by desmosterol accumulation and ^{13}C labelling of cholesterol. In our preclinical mouse model, we did not observe adverse effects of SH42 treatment on food intake, body

weight, and body composition. Additionally, desmosterol-induced LXR activation via inhibition of DHCR24 did not cause a reduction of circulating neutrophils or neutropenia, another adverse effect of systemic LXR activation [27]. Importantly, our study showed that DHCR24 inhibition by SH42 not only prevented, but also affected NASH progression in mice with established hepatic steatosis, as evidenced by reducing the number of hepatic crown-like structures, collagen content and plasma alanine transaminase levels. These advantages of targeting DHCR24 over synthetic LXR agonists will possibly lead to a promising application of DHCR24 inhibitors to combat NAFLD/NASH, in addition to other cardiometabolic and inflammatory diseases. Of note, our study is limited by our inability to provide direct evidence of SH42 binding to DHCR24, due to a lack of available pure enzyme and the fact that DHCR24 is membrane bound making its isolation and co-crystallization very difficult. Therefore, we cannot exclude that SH42 exerts indirect inhibitory actions responsible for desmosterol accumulation or interaction with yet undiscovered targets contributing to the improvement of the NAFLD phenotype in our study.

In conclusion, we show that pharmacological inhibition of DHCR24 increases desmosterol to prevent diet-induced hepatic steatosis and inflammation, two main hallmarks of NAFLD/NASH development, without inducing hyperlipidemia. As such, our study paves the way for developing a new therapeutic strategy for the treatment for NAFLD/NASH.

Acknowledgements

This work was supported by the Netherlands Organisation for Health Research and Development-ZonMW (Early Career Scientist Hotel grant 435004007 to Y.W.); the National Natural Science Foundation of China (grant 82170876 to Y.W.); the Netherlands Cardiovascular Research Initiative: an initiative with support of the Dutch Heart Foundation (CVON-GENIUS-2 to P.C.N.R., CVON-IN CONTROL-2 to F.K.); and the Netherlands Heart Foundation (2009T038 to P.C.N.R.); the Department of Science and Technology Foundation of Shaanxi province (2021SF-021 to Y.W.). the Department of Science and Technology Foundation of Shaanxi province (2021SF-021 to Y.W.). M.G. was partially supported by the Netherlands X-omics initiative which is partially funded by NWO, project 184.034.019. Y.W. is supported by the China “Thousand Talents Plan” (Young Talents), Shaanxi province “Thousand Talents Plan” (Young Talents) and Foundation of Xi’an Jiaotong University (Plan A).

Author Contributions

Enchen Zhou: Conceptualization, data curation, formal analysis, investigation, visualization, methodology, writing – original draft, project administration, writing – review and editing; Xiaoke Ge: formal analysis, investigation, methodology, writing – review and editing; Hiroyuki Nakashima: conceptualization, data curation, formal analysis, investigation, visualization, methodology, writing – review and editing; Rumei Li: formal analysis, investigation, methodology, writing – review and editing; Hendrik J. P. van der Zande: formal analysis, investigation, methodology, writing – review and editing; Cong Liu: investigation, writing – review and editing; Zhuang Li: investigation, writing – review and editing; Christoph Müller: resources, writing – review and editing; Franz Bracher: resources, writing – review and editing; Yassene Mohammed: data curation, formal analysis, visualization, writing – review and editing; Jan Freark de Boer: investigation, project administration, writing – review and editing; Folkert Kuipers: resources, project administration, writing – review and editing; Bruno Guigas: resources, project administration, writing – review and editing; Christopher K. Glass: resources, supervision, project administration, writing – review and editing; Patrick C. N. Rensen: conceptualization, resources, data curation, supervision, funding acquisition, project administration, writing – review and editing; Martin Giera: conceptualization, resources, data curation, supervision, funding acquisition, project administration, writing – review and editing; Yanan Wang: conceptualization, resources, data curation, supervision, funding acquisition, project administration, writing – review and editing.

Disclosure Statement & Competing Interests

The authors have no conflicts of interest to disclose.

Data Availability

The authors declare that all data supporting the findings of this study are available within the paper and its supplementary information appendix. This study includes no data deposited in external repositories.

References

1. Berlanga A., Guiu-Jurado E., Porras J. A.*, et al.* Molecular pathways in non-alcoholic fatty liver disease. *Clin Exp Gastroenterol* **7**, 221–239 (2014).
2. Chalasani N., Younossi Z., Lavine J. E.*, et al.* The diagnosis and management of nonalcoholic fatty liver disease: Practice guidance from the American Association for the Study of Liver Diseases. *Hepatology* **67**, 328–357 (2018).
3. Riazi K., Azhari H., Charette J. H.*, et al.* The prevalence and incidence of NAFLD worldwide: a systematic review and meta-analysis. *Lancet Gastroenterol Hepatol* **7**, 851–861 (2022).
4. Baffy G. Kupffer cells in non-alcoholic fatty liver disease: the emerging view. *J Hepatol* **51**, 212–223 (2009).
5. Wandrer F., Liebig S., Marhenke S.*, et al.* TNF-Receptor-1 inhibition reduces liver steatosis, hepatocellular injury and fibrosis in NAFLD mice. *Cell Death Dis* **11**, 212 (2020).
6. Aparicio-Vergara M., Hommelberg P. P., Schreurs M.*, et al.* Tumor necrosis factor receptor 1 gain-of-function mutation aggravates nonalcoholic fatty liver disease but does not cause insulin resistance in a murine model. *Hepatology* **57**, 566–576 (2013).
7. Schuster S., Cabrera D., Arrese M.*, et al.* Triggering and resolution of inflammation in NASH. *Nat Rev Gastroenterol Hepatol* **15**, 349–364 (2018).
8. Tosello-Trampont A. C., Landes S. G., Nguyen V.*, et al.* Kuppfer cells trigger nonalcoholic steatohepatitis development in diet-induced mouse model through tumor necrosis factor-alpha production. *The Journal of biological chemistry* **287**, 40161–40172 (2012).
9. Huang W., Metlakunta A., Dedousis N.*, et al.* Depletion of liver Kupffer cells prevents the development of diet-induced hepatic steatosis and insulin resistance. *Diabetes* **59**, 347–357 (2010).
10. Lanthier N., Molendi-Coste O., Cani P. D.*, et al.* Kupffer cell depletion prevents but has no therapeutic effect on metabolic and inflammatory changes induced by a high-fat diet. *FASEB J* **25**, 4301–4311 (2011).
11. Bieghs V., Walenbergh S. M., Hendrikx T.*, et al.* Trapping of oxidized LDL in lysosomes of Kupffer cells is a trigger for hepatic inflammation. *Liver Int* **33**, 1056–1061 (2013).
12. Tran S., Baba I., Poupel L.*, et al.* Impaired Kupffer Cell Self-Renewal Alters the Liver Response to Lipid Overload during Non-alcoholic Steatohepatitis. *Immunity* **53**, 627–640 e625 (2020).
13. Remmerie A., Martens L., Thone T.*, et al.* Osteopontin Expression Identifies a Subset of Recruited Macrophages Distinct from Kupffer Cells in the Fatty Liver. *Immunity* **53**, 641–657 e614 (2020).
14. Seidman J. S., Troutman T. D., Sakai M.*, et al.* Niche-Specific Reprogramming of Epigenetic Landscapes Drives Myeloid Cell Diversity in Nonalcoholic Steatohepatitis. *Immunity* **52**, 1057–1074 e1057 (2020).
15. Ito A., Hong C., Rong X.*, et al.* LXRs link metabolism to inflammation through Abca1-dependent regulation of membrane composition and TLR signaling. *Elife* **4**, e08009 (2015).
16. Bensinger S. J., Tontonoz P. Integration of metabolism and inflammation by lipid-activated nuclear receptors. *Nature* **454**, 470–477 (2008).
17. Prufer K., Boudreaux J. Nuclear localization of liver X receptor alpha and beta is differentially regulated. *J Cell Biochem* **100**, 69–85 (2007).
18. Venkateswaran A., Laffitte B. A., Joseph S. B.*, et al.* Control of cellular cholesterol efflux by the nuclear oxysterol receptor LXR alpha. *Proceedings of the National Academy of Sciences of the United States of America* **97**, 12097–12102 (2000).

19. Bischoff E. D., Daige C. L., Petrowski M.*, et al.* Non-redundant roles for LXRalpha and LXRbeta in atherosclerosis susceptibility in low density lipoprotein receptor knockout mice. *J Lipid Res* **51**, 900–906 (2010).
20. Ishibashi M., Filomenko R., Rebe C.*, et al.* Knock-down of the oxysterol receptor LXRalpha impairs cholesterol efflux in human primary macrophages: lack of compensation by LXRbeta activation. *Biochem Pharmacol* **86**, 122–129 (2013).
21. Joseph S. B., Bradley M. N., Castrillo A.*, et al.* LXR-dependent gene expression is important for macrophage survival and the innate immune response. *Cell* **119**, 299–309 (2004).
22. Wang Y. Y., Dahle M. K., Agren J.*, et al.* Activation of the liver X receptor protects against hepatic injury in endotoxemia by suppressing Kupffer cell activation. *Shock* **25**, 141–146 (2006).
23. Li P., Spann N. J., Kaikkonen M. U.*, et al.* NCoR repression of LXRs restricts macrophage biosynthesis of insulin-sensitizing omega 3 fatty acids. *Cell* **155**, 200–214 (2013).
24. Korner A., Zhou E., Muller C.*, et al.* Inhibition of Delta24-dehydrocholesterol reductase activates pro-resolving lipid mediator biosynthesis and inflammation resolution. *Proc Natl Acad Sci U S A* **116**, 20623–20634 (2019).
25. Grefhorst A., Elzinga B. M., Voshol P. J.*, et al.* Stimulation of lipogenesis by pharmacological activation of the liver X receptor leads to production of large, triglyceride-rich very low density lipoprotein particles. *J. Biol. Chem.* **277**, 34182–34190 (2002).
26. Schultz J. R., Tu H., Luk A.*, et al.* Role of LXRs in control of lipogenesis. *Genes Dev.* **14**, 2831–2838 (2000).
27. Kirchgessner T. G., Sleph P., Ostrowski J.*, et al.* Beneficial and Adverse Effects of an LXR Agonist on Human Lipid and Lipoprotein Metabolism and Circulating Neutrophils. *Cell metabolism* **24**, 223–233 (2016).
28. Spann N. J., Garmire L. X., McDonald J. G.*, et al.* Regulated accumulation of desmosterol integrates macrophage lipid metabolism and inflammatory responses. *Cell* **151**, 138–152 (2012).
29. Muse E. D., Yu S., Edillor C. R.*, et al.* Cell-specific discrimination of desmosterol and desmosterol mimetics confers selective regulation of LXR and SREBP in macrophages. *Proc. Natl. Acad. Sci. U. S. A.* **115**, E4680–e4689 (2018).
30. Nes W. D. Biosynthesis of cholesterol and other sterols. *Chem Rev* **111**, 6423–6451 (2011).
31. Muller C., Hemmers S., Bartl N.*, et al.* New chemotype of selective and potent inhibitors of human delta 24-dehydrocholesterol reductase. *Eur J Med Chem* **140**, 305–320 (2017).
32. Westerterp M., van der Hoogt C. C., de Haan W.*, et al.* Cholesteryl ester transfer protein decreases high-density lipoprotein and severely aggravates atherosclerosis in APOE*3-Leiden mice. *Arterioscler Thromb Vasc Biol* **26**, 2552–2559 (2006).
33. Tarasco E., Pellegrini G., Whiting L.*, et al.* Phenotypical heterogeneity in responder and nonresponder male ApoE*3Leiden.CETP mice. *Am J Physiol Gastrointest Liver Physiol* **315**, G602–G617 (2018).
34. Plosch T., van der Veen J. N., Havinga R.*, et al.* Abcg5/Abcg8-independent pathways contribute to hepatobiliary cholesterol secretion in mice. *Am J Physiol Gastrointest Liver Physiol* **291**, G414–423 (2006).
35. Matthews D. R., Hosker J. P., Rudenski A. S.*, et al.* Homeostasis model assessment: insulin resistance and beta-cell function from fasting plasma glucose and insulin concentrations in man. *Diabetologia* **28**, 412–419 (1985).
36. Liang W., Menke A. L., Driessen A.*, et al.* Establishment of a general NAFLD scoring system for rodent models and comparison to human liver pathology. *PLoS One* **9**, e115922 (2014).
37. Itoh M., Kato H., Suganami T.*, et al.* Hepatic crown-like structure: a unique histological feature in non-alcoholic steatohepatitis in mice and humans. *PLoS One* **8**, e82163 (2013).

38. Hussaarts L., Garcia-Tardon N., van Beek L.*, et al.* Chronic helminth infection and helminth-derived egg antigens promote adipose tissue M2 macrophages and improve insulin sensitivity in obese mice. *FASEB J* **29**, 3027–3039 (2015).
39. Peet D. J., Turley S. D., Ma W.*, et al.* Cholesterol and bile acid metabolism are impaired in mice lacking the nuclear oxysterol receptor LXR alpha. *Cell* **93**, 693–704 (1998).
40. Endo-Umeda K., Nakashima H., Umeda N.*, et al.* Dysregulation of Kupffer Cells/Macrophages and Natural Killer T Cells in Steatohepatitis in LXRalpha Knockout Male Mice. *Endocrinology* **159**, 1419–1432 (2018).
41. Endo-Umeda K., Makishima M. Liver X Receptors Regulate Cholesterol Metabolism and Immunity in Hepatic Nonparenchymal Cells. *Int J Mol Sci* **20**, (2019).
42. Rodríguez-Acebes S., de la Cueva P., Fernández-Hernando C.*, et al.* Desmosterol can replace cholesterol in sustaining cell proliferation and regulating the SREBP pathway in a sterol-Delta24-reductase-deficient cell line. *Biochem. J.* **420**, 305–315 (2009).
43. Snodgrass R. G., Benatzy Y., Schmid T.*, et al.* Efferocytosis potentiates the expression of arachidonate 15-lipoxygenase (ALOX15) in alternatively activated human macrophages through LXR activation. *Cell Death Differ*, (2020).
44. Lavin Y., Winter D., Blecher-Gonen R.*, et al.* Tissue-resident macrophage enhancer landscapes are shaped by the local microenvironment. *Cell* **159**, 1312–1326 (2014).
45. Hirsova P., Gores G. J. Death Receptor-Mediated Cell Death and Proinflammatory Signaling in Nonalcoholic Steatohepatitis. *Cell Mol Gastroenterol Hepatol* **1**, 17–27 (2015).
46. Bieghs V., van Gorp P. J., Walenbergh S. M.*, et al.* Specific immunization strategies against oxidized low-density lipoprotein: a novel way to reduce nonalcoholic steatohepatitis in mice. *Hepatology* **56**, 894–903 (2012).
47. Liu L., Mei M., Yang S.*, et al.* Roles of chronic low-grade inflammation in the development of ectopic fat deposition. *Mediators Inflamm* **2014**, 418185 (2014).
48. Bradley M. N., Hong C., Chen M.*, et al.* Ligand activation of LXR beta reverses atherosclerosis and cellular cholesterol overload in mice lacking LXR alpha and apoE. *The Journal of clinical investigation* **117**, 2337–2346 (2007).
49. Zhang Y., Breevoort S. R., Angdisen J.*, et al.* Liver LXRalpha expression is crucial for whole body cholesterol homeostasis and reverse cholesterol transport in mice. *The Journal of clinical investigation* **122**, 1688–1699 (2012).
50. Simonen M., Mannisto V., Leppanen J.*, et al.* Desmosterol in human nonalcoholic steatohepatitis. *Hepatology* **58**, 976–982 (2013).
51. Sliz E., Shin J., Syme C.*, et al.* A variant near DHCR24 associates with microstructural properties of white matter and peripheral lipid metabolism in adolescents. *Mol Psychiatry*, (2020).
52. Müller C., Junker J., Bracher F.*, et al.* A gas chromatography-mass spectrometry-based whole-cell screening assay for target identification in distal cholesterol biosynthesis. *Nat. Protoc.* **14**, 2546–2570 (2019).
53. Kirby T. J. Cataracts produced by triparanol. (MER-29). *Trans Am Ophthalmol Soc* **65**, 494–543 (1967).
54. Moebius F. F., Fitzky B. U., Lee J. N.*, et al.* Molecular cloning and expression of the human delta7-sterol reductase. *Proceedings of the National Academy of Sciences of the United States of America* **95**, 1899–1902 (1998).

Expanded View Figures

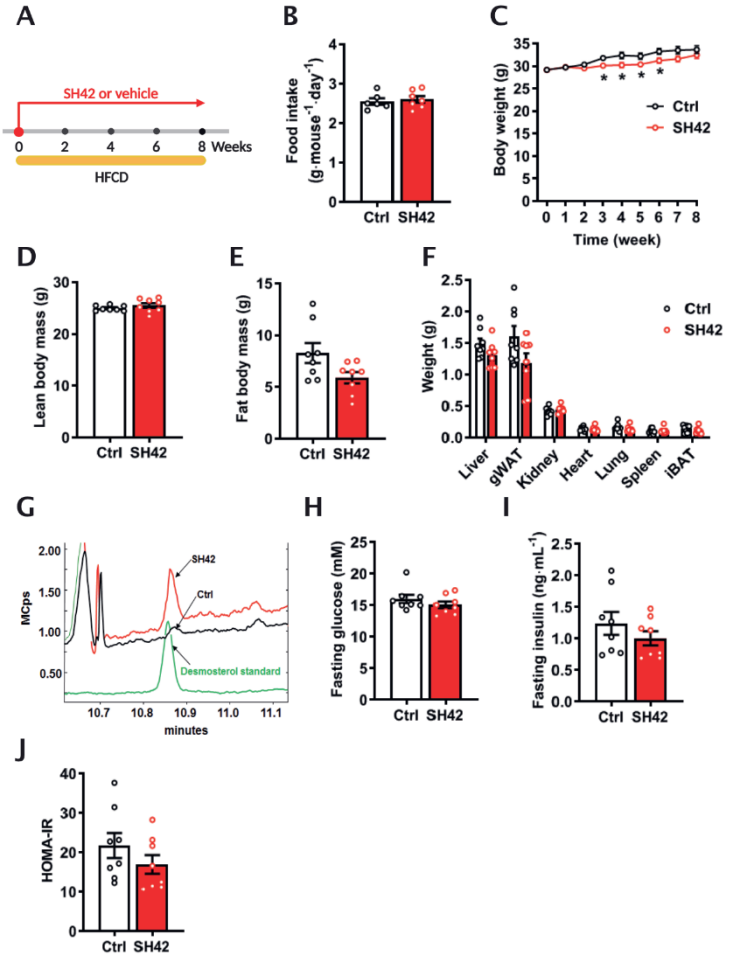

Fig. EV1. Inhibition of DHCR24 by SH42 does not affect food intake, body composition, organ weight, and plasma glucose and insulin levels, while increasing plasma desmosterol levels. (**A**) *E3L.CETP* mice fed a high fat high cholesterol diet (HFCD) were treated with vehicle (Ctrl) or DHCR24 inhibitor SH42 (SH42) (n= 8 mice per group). (**B**) Food intake was measured during week 3 to 6 (n= 6 and 7 cages, respectively). (**C**) Body weight was measured weekly and (**D**) lean body mass and (**E**) fat body mass were determined at the end of week 8. (**F**) After 8 weeks of treatment, mice were killed and organs were collected and weighted. Four hour-fasted blood samples were collected before the sacrifice to measure (**G**) desmosterol levels and (**H**) glucose and (**I**) insulin levels. (**J**) The homeostatic Model Assessment for Insulin Resistance (HOMA-IR) scores were calculated. Data information: Values are mean ± SEM. Differences between two groups (SH42/Ctrl) were determined using a non-parametric Mann-Whitney test. Abbreviations: gWAT, gonadal white adipose tissue; iBAT, interscapular brown adipose tissue.

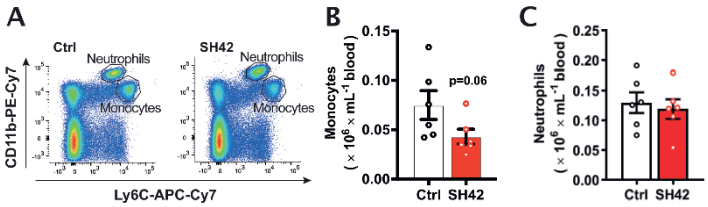

Fig. EV2. Inhibition of DHCR24 by SH42 tends to reduce circulating monocytes while no effect on circulating neutrophils. *E3L.CETP* mice fed a HFCD were treated with vehicle (Ctrl) or DHCR24 inhibitor SH42 (SH42) (n= 6 mice per group). After 4 weeks of treatment, blood samples were collected to measure (**A**, **B**) monocytes and (**A**, **C**) neutrophils via flow cytometry. Values are mean ± SEM. Differences between two groups (SH42/Ctrl) were determined using a non-parametric Mann-Whitney test.

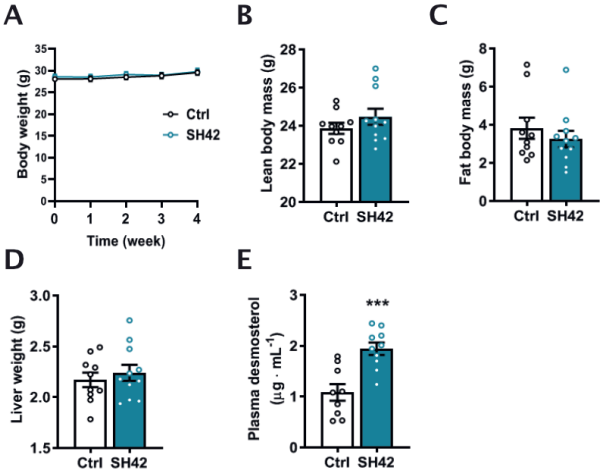

Fig. EV3. Inhibition of DHCR24 by SH42 does not affect body weight, body composition or liver weight, while increasing plasma desmosterol levels in LXRα-deficient mice. LXRα deficient mice fed HFCD were treated with vehicle (Ctrl) or DHCR24 inhibitor SH42 (SH42) (n= 10 and 11 mice, respectively). (**A**) Body weight was measured weekly. After 4 weeks of treatment, (**B**) lean body mass and (**C**) fat body mass were determined. (**D**) Mice were killed and livers were collected and weighted. (**E**) Plasma desmosterol levels were measured at the end of the experiment (n= 9 and 11 mice respectively; one sample in control group was lost due to technical failure). Data information: Values are mean ± SEM. Differences between two groups (SH42/Ctrl) were determined using a non-parametric Mann-Whitney test. ***P<0.001 vs. ctrl.

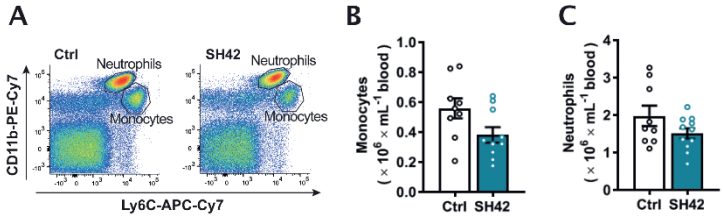

Fig. EV4. Inhibition of DHCR24 by SH42 does affect circulating monocytes and neutrophils in LXRα-deficient mice. LXRα deficient mice fed HFCD were treated with vehicle (Ctrl) or DHCR24 inhibitor SH42 (SH42) (n= 10 and 11 mice respectively). After 4 weeks of treatment, blood samples were collected to measure (**A**, **B**) monocytes (n= 9 and 10 mice respectively; two values were identified as outliers based on Grubbs' test and removed from statistical analysis) and (**A**, **C**) neutrophils were determined (n= 9 and 11 mice respectively; one value was identified as an outlier based on Grubbs' test and removed from statistical analysis) via flow cytometry analysis. Values are mean ± SEM. Differences between two groups (SH42/Ctrl) were determined using a non-parametric Mann-Whitney test.

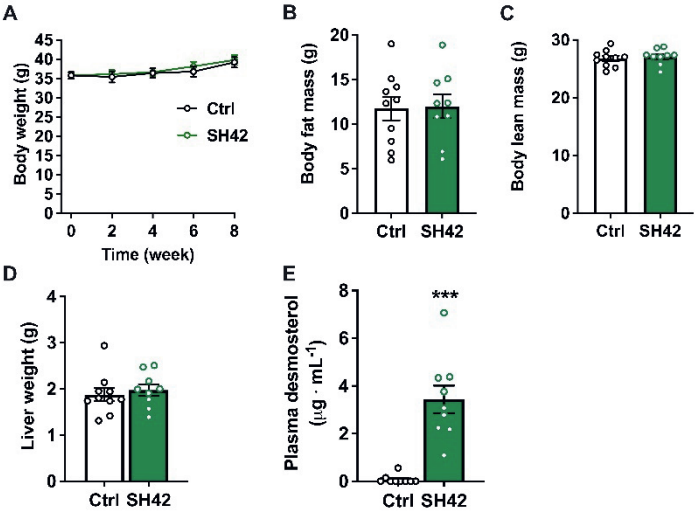

Fig. EV5. Inhibition of DHCR24 by SH42 increases plasma desmosterol and does not influence body and liver weight after 10 weeks of HFCD treatment. *E3L.CETP* mice were fed with a HFCD for 10 weeks first and then treated with vehicle (Ctrl) or DHCR24 inhibitor SH42 (SH42) (n= 10 and 9 mice, respectively) for additional 8 weeks. (**A**) Body weight was measured at indicated time points. After the 18 weeks, (**B**) lean and (**C**) fat body mass was evaluated. Mice were killed and (**D**) liver weight and (**E**) plasma desmosterol levels were measured. Data information: Values are mean ± SEM. Differences between two groups (SH42/Ctrl) were determined using a non-parametric Mann-Whitney test. ***p<0.001 vs. control (ctrl).

Appendix Figures and Tables

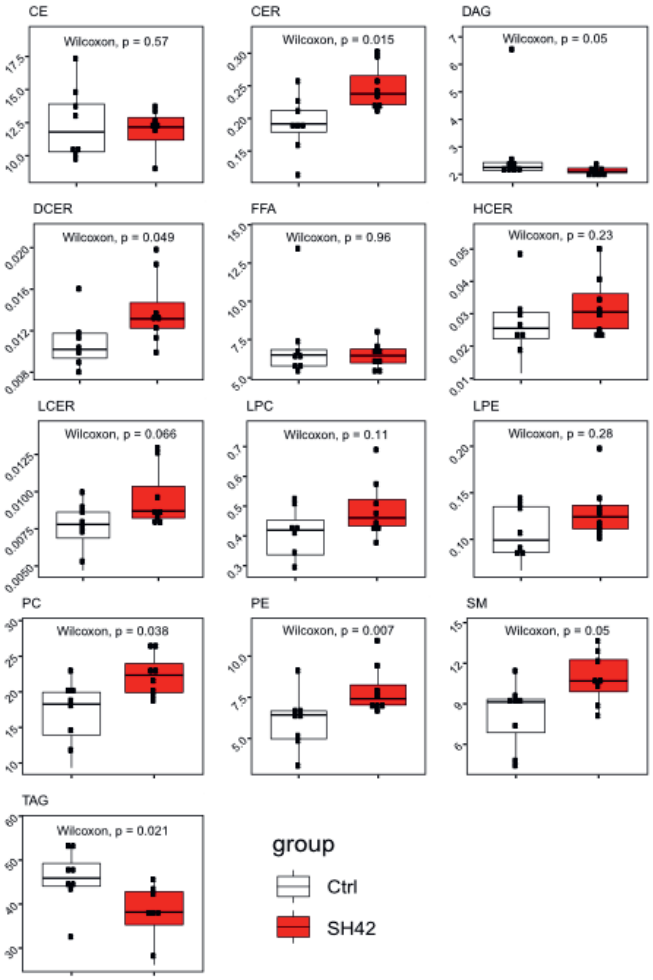

Appendix Fig. S1. Inhibition of DHCR24 by SH42 alters liver lipid class compositions. *E3L.CETP* mice fed a HFCD were treated with vehicle (Ctrl) or DHCR24 inhibitor SH42 (SH42) (n= 8 mice per group). After 8 weeks of treatment, mice were killed and livers were collect to determine liver lipid class compositions. The boxplot indicates 1st quartile, median, and 3rd quartile. Differences between two groups (SH42/Ctrl) were determined using Wilcoxon rank sum test. Abbreviations: CE, cholesteryl esters; CER, ceramides; DAG, diacylglycerols; DCER, dihydroceramides; FFA, free fatty acids; HCER, hexosylceramides; LPC, lysophosphatidylcholines; LPE, lysophosphatidylethanolamines; PC, phosphatidylcholines; PE, phosphatidylethanolamines; SM, sphingomyelins; TAG, triacylglycerols.

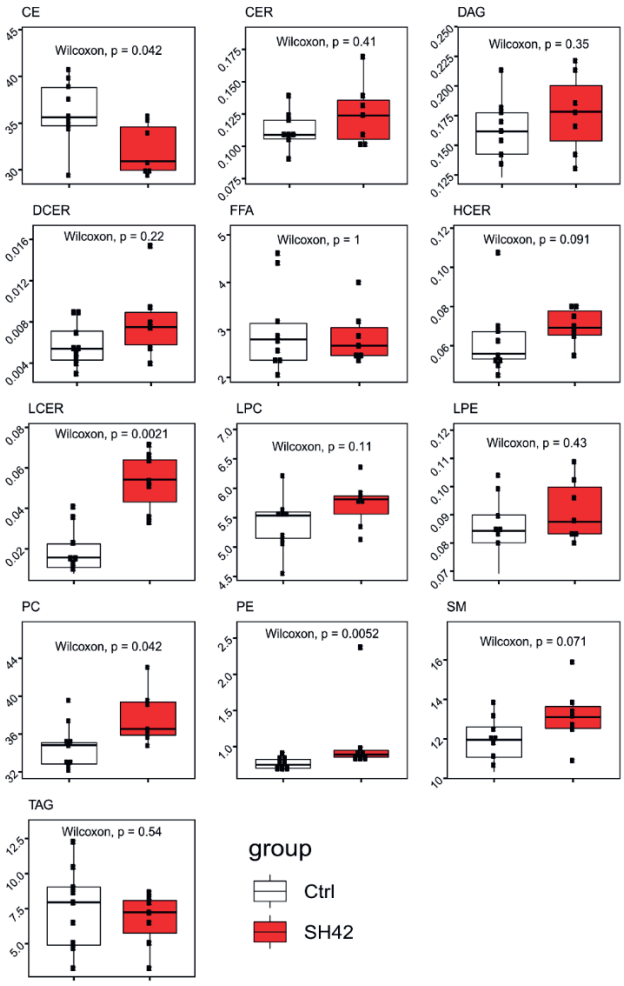

Appendix Fig. S2. Inhibition of DHCR24 by SH42 does not increase plasma DAG and TAG fractions. *E3L.CETP* mice fed a HFCD were treated with vehicle (Ctrl) or DHCR24 inhibitor SH42 (SH42) (n= 8 mice per group). After 8 weeks of treatment, blood samples were collected to determine lipid class compositions. The boxplot indicates 1st quartile, median, and 3rd quartile. Differences between two groups (SH42/Ctrl) were determined using Wilcoxon rank sum test. Abbreviations: CE, cholesteryl esters; CER, ceramides; DAG, diacylglycerols; DCER, dihydroceramides; FFA, free fatty acids; HCER, hexosylceramides; LPC, lysophosphatidylcholines; LPE, lysophosphatidylethanolamines; PC, phosphatidylcholines; PE, phosphatidylethanolamines; SM, sphingomyelins; TAG, triacylglycerols.

Appendix Fig. S3. Representative gating scheme for FACS analysis in liver samples

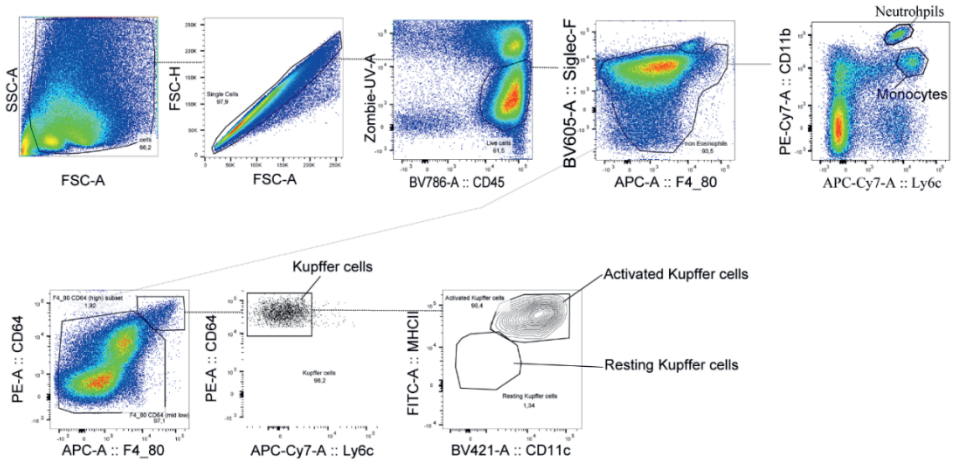

Appendix Fig. S4. Representative gating scheme for FACS analysis in blood samples

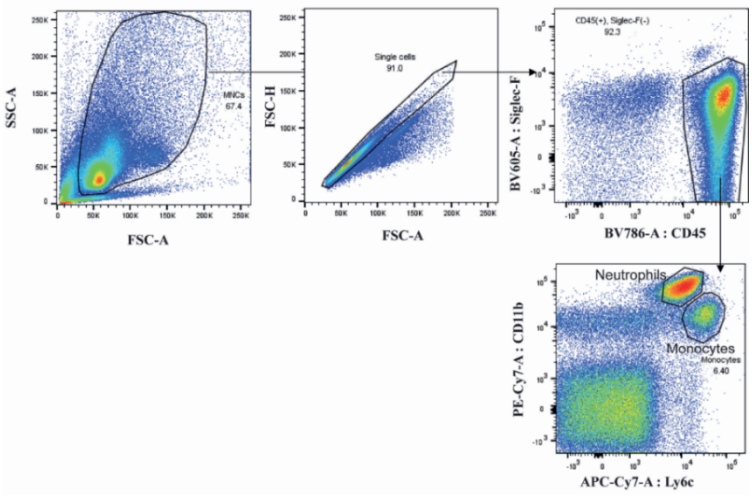

Appendix Table S1. Antibodies used for immunohistochemistry

Target	Concentration used	Vendor	Catalog No.
F4/80	1 µg·mL-1	Serotec, Oxford, UK	MCA497

Appendix Table S2. Antibodies used for flow cytometry

Fluorophore	Target	Clone	Vendor
FITC	MHCII	M5/114.15.2	Biolegend
PE	CD64	X54-5/7.1	Biolegend
PE-Cy7	CD11b	M1/70	eBioscience
APC	F4/80	BM8	eBioscience
APC-Cy7	Ly6C	HK1.4	Biolegend
BV421	CD11c	N418	Biolegend
BV605	Siglec-F	E50-2440	BD Biosciences
BV785	CD45	30F11	Biolegend